Lab on a Chip

Accepted Manuscript

ROYAL SOCIETY OF CHEMISTRY

www.rsc.org/loc

Size and Deformability based Separation of Circulating Tumor Cells from Castrate Resistant Prostate Cancer Patients using Resettable Cell Traps

Xi Qin[a], Sunyoung Park[a], Simon P. Duffy[a], Kerryn Matthews[a], Richard R. Ang[a], Tilman Todenhöfer[b], Hamid Abdi[b], Arun Azad[c], Jenny Bazov[b], Kim N. Chi[abc], Peter C. Black[ab], and Hongshen Ma[ab]

a Department of Mechanical Engineering, University of British Columbia, 2054-6250 Applied Science Lane, Vancouver, BC, Canada V6T 1Z4
b Vancouver Prostate Centre, Vancouver General Hospital, Vancouver, BC, Canada
c BC Cancer Agency – Vancouver Cancer Centre, Vancouver General Hospital, Vancouver, BC, Canada

ABSTRACT

The enumeration and capture of circulating tumor cells (CTCs) are potentially of great clinical value by offering a non-invasive means to access tumor materials to diagnose disease and monitor treatment efficacy. Conventional immunoenrichment of CTCs may fail to capture cells with low surface antigen expression. Micropore filtration presents a compelling label-free alternative that enriches for CTCs using their biophysical rather than biochemical characteristics. However, this strategy is prone to clogging of the filter microstructure, which dramatically reduces selectivity after processing large numbers of cells. Here, we use the resettable cell trap (RCT) mechanism to separate cells based on their size and deformability using an adjustable aperture that can be periodically cleared to prevent clogging. After separation, the output sample is stained and analyzed using multi-spectral analysis, which provides a more sensitive and unambiguous method to identify CTC biomarkers than traditional immunofluorescence. We tested the RCT device using blood samples obtained from 22 patients with metastatic castrate-resistant prostate cancer while comparing the results with the established CellSearch® system. The RCT mechanism was able to capture ≥5 CTCs in 18/22 (82%) patients with a mean count of 257 in 7.5 ml of whole blood, while the CellSearch system found ≥5 CTCs in 9/22 (38%) patients with a mean count of 25. The ~10X improvement in CTC capture rate provides significant more materials for subsequent analysis of these cells such as immunofluorescence, propagation by tissue culture, and genetic profiling.

INTRODUCTION

Circulating tumor cells (CTCs) are cells from primary or metastatic tumor sites that are shed into the peripheral blood circulation. The enumeration and capture of CTCs in blood potentially has clinical value by offering a non-invasive means to diagnose the presence of tumors, to monitor treatment efficacy and to study evolving molecular alterations under therapy[1–3]. Correlation between CTC counts and both progression and overall survival have been reported in patients with various metastatic cancers [4–8]. Current CTC separation platforms can be stratified into methods that involve biochemical selection and biophysical selection [9]. Biochemical methods typically discriminate tumor cells from leukocytes based on the expression of surface antigens such as the epithelial cell adhesion molecule (EpCAM). This approach is currently employed by the CellSearch system (Janssen Diagnostics, USA), the only FDA-approved commercial system for CTC enumeration, as well as many research systems currently in development[10–13]. A key limitation of this approach is the potential to miss CTCs because of the variability in the cell surface markers for positive selection that prevent the efficient capture of CTCs. This loss can arise in two ways: first, the heterogeneity of CTCs results in different expression levels of surface markers among different cancer types and even within the same patient [1,14]. Second, due to the epithelial to mesenchymal transition (EMT), a subpopulation of CTCs, which are potentially highly aggressive, are thought to lose expression of epithelial antigens [15].

To compensate for this potential loss, recent research in this field has focused on label-free separation of CTCs, based on differences in their biophysical properties relative to leukocytes. One approach is micropore filtration which separates CTCs from hematological cells based on differences in size and deformability [16,17]. A key challenge of this approach is clogging of the filter microstructures, which occurs after processing a large number of cells. Clogging causes unpredictable changes of the hydrodynamic resistance of the filter resulting in reduced selectivity. Additionally, the retrieval of isolated CTCs is often difficult or impossible since these methods typically trap and identify the captured cells on-chip, but cannot release them for subsequent analysis [16–19].

We previously developed a mechanism for chromatographic separation of cells based on their physical differences using the transit speed of cells through a textured microfluidic [20]. We then generalized this method to create the resettable cell trap (RCT) mechanism, which uses an adjustable aperture to capture cells based on their size and deformability, and can be periodically cleared to prevent clogging [21]. Here, we developed an enhanced multiplexed version of this mechanism with improved selectivity and

throughput. This new chip successfully demonstrates high-sensitivity separation of CTCs from whole blood of patients with metastatic castration-resistant prostate cancer (mCRPC). Unlabeled and viable CTCs separated from patient blood samples were retrieved, identified via immunostaining, and could be extracted for downstream analysis.

DESIGN

Resettable Cell Trap Mechanism

The resettable cell trap is a two-layer PDMS structure comprising a sample-carrying upper flow channel and a lower fluid-filled control channel. Separating these two layers is a thin flexible diaphragm that can be inflated by applying an external pneumatic pressure to control the geometry of the two microchannels. Opposing the diaphragm, the surface of the flow channel is textured with two rows of micro-pockets and a protruding center fin (Figure 1A). These microstructures and the diaphragm combines to create an adjustable aperture that selectively traps and releases target cells. The position of the diaphragm can be considered to have two states: a constricted state, where the diaphragm is in contact with the textured surface to reduce the aperture of the flow channel; as well as a relaxed state, where the diaphragm is deflected away from the textured surface to enlarge the aperture of the flow channel (Figure 1A).

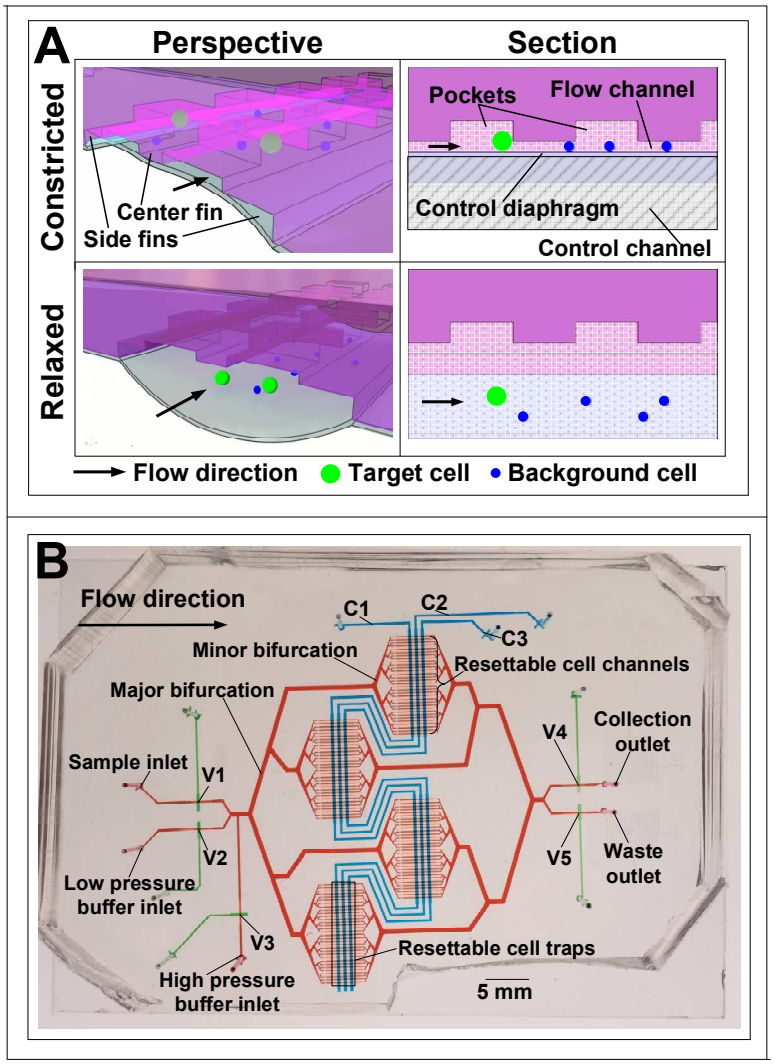

Figure 1:The resettable cell trap. A: In the constricted state, the flow channel and diaphragm form an aperture to capture the more rigid target cells. In the relaxed state, target cells can be released and collected and the device is reset to its original state. B: Photograph of the multiplexed microfluidic device. The red filled channels are flow and resettable cell channels carrying sample. The blue filled channels (C1-C3) are the adjustable control diaphragms that trap the cells in the resettable cell traps (darker blue). The green filled channels (V1-V5) form the on/off valves that control the flow of sample.

In the constricted state, the pressure in the control channel is greater than the flow channel and the diaphragm is deflected to come into contact with the center and side fins of the flow channel. The center fin and the two side fins act as the mechanical stop to limit the movement of the diaphragm and flatten it to create an approximately rectangular channel on either side of the center fin with a minimum size of 5 µm. Since the top and bottom boundary of the aperture is the most parallel at the center of the

channel, a flow focuser is used to center the cells upstream in the flow channels to provide a consistent filtration aperture for the incoming cell stream [21]. Furthermore, multiple micro-pockets at the trap area line both sides of the center fin and temporarily hold the larger and more rigid cells to prevent them from blocking the flow channel. This structure is capable of selectively capturing cells based on their phenotypically distinct size and deformability.

In the relaxed state, the pressure in the control channel is less than the flow channel and the diaphragm is deflected away from the textured surface of the flow channel. The aperture in this state is large enough for all cells to pass through freely. By simply relaxing the diaphragm, the micro-pockets filled with captured cells can be purged to empty the recesses and the channels are reset. This ability to refresh the flow channel on demand is important to release captured cells and prevent clogging.

One of the key advantages of the RCT mechanism is its ability to create an adjustable aperture with well-controlled geometry inside a microchannel. Previous adjustable mechanisms have employed only the basic structure of the conventional rectangular membrane micro-valves, [22] which, when the diaphragm is inflated, form two triangular openings at the two upper corners of the flow channel to close it off. These triangular pores do not provide a well-controlled shape and therefore cannot provide a precisely controlled aperture for separating cells. Consequently, these mechanisms have been restricted to the separation of particles from suspension [23]. The RCT mechanism enables a precisely controlled separation aperture by adding a center fin and two side fins to a rectangular microchannel. When deflected, the flexible diaphragm is bisected by the center fin and flattens to make two rectangular channels with a rectangular aperture that could be used to specifically select cells based on a combination of size and deformability. Previously, we showed that this mechanism is capable of separating polymer microbeads with less than 1 µm resolution and that whole blood could be filtered with a throughput of ~900,000 nucleated cells per hour [21].

Device Operation

As shown in Figure 1B, the improved RCT device consists of 4 groups of 32 parallelized (128 channels in total) resettable cell channels (shown in red) with 3 control diaphragm channels (C1-C3, shown in blue) that make up 3 x 128 resettable cell traps (shown in darker blue). Bifurcation channels (minor and major) are designed to connect the 128 channels and to evenly distribute cells into each cell trap channel[24]. Five

on/off valves (V1-V5, shown in green) route the sample and buffers from inlet reservoirs into the collection and waste reservoirs as required[22].

Cell separation using this device involves a three-step cycle of filtration, purging, and collection. The filtration step (Figure 2, Step 1) involves infusing cells from the sample inlet into the constricted cell trap. The cell traps catch the larger and more rigid target cells while the smaller and less rigid leukocytes traverse through to the waste reservoir. The purging step (Figure 2, Step 2) involves infusing buffer fluid at a modest pressure while the cell trap is constricted. This process washes away the contaminant leukocytes remaining in the cell traps. The collection step (Figure 2, Step 5) involves infusing buffer fluid at a higher pressure with all the cell traps opened. All of the cells that are captured are released and directed into the collection reservoir. This releasing flow is much faster than the filtration and purging flow so as to produce high shear forces to remove cells that may have adhered to the walls of the cell traps [25,26]. The filtration step lasts 10 minutes, the purging step takes 5-10 seconds and the collection step lasts 2-3 seconds. After the collection step, all cells are removed from the trap area and the device is reset back to its initial state. This periodic refresh process prevents clogging and fouling to maintain selectivity of the separation mechanism, and thereby allowing the filtration process to continue perpetually.

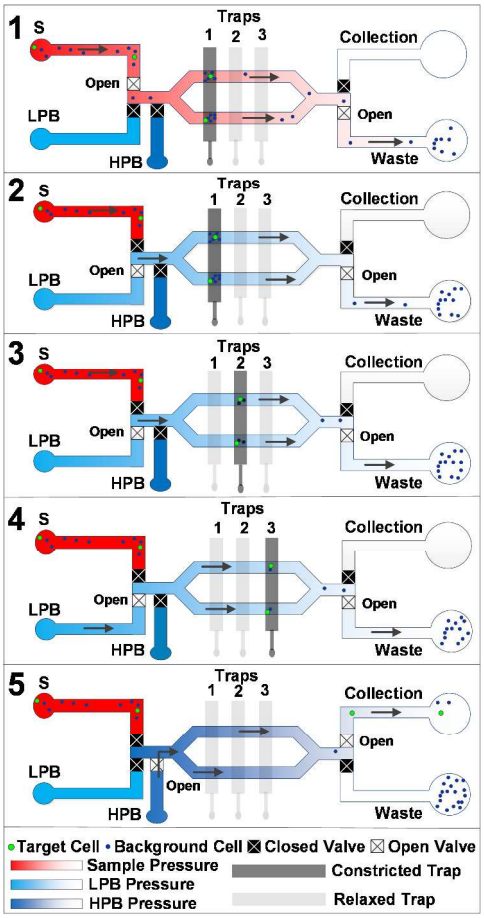

Figure 2: Cells from the inlet are filtered through three resettable cell traps before being flowed to the collection outlet. Captured cells are purged using a low-pressure buffer (LPB) flow, and collected with high-pressure buffer (HPB) flow. Step 1 is the initial filtration. Step 2 is the purging step. Step 3 & 4 are the 2x re-filtration steps and Step 5 is the collection step.

Multi-filtration

In early experiments it was observed that cancer cells were primarily captured in the micro-pockets at the beginning of the constricted trap while white blood cells (WBCs) were captured on surfaces throughout the micro-pockets in the entire cell trap microstructure. This behavior suggests that cancer cells are captured because of mechanical constraint while leukocytes are captured because of non-specific adsorption. Interestingly, leukocytes that have adsorbed onto the walls of the cell traps can be released using greater shear stress applied through increased flow rate in the collection step, which suggests the potential to improve selectivity by filtering a sample multiple times. To investigate this

possibility, we cascaded three identical resettable cell traps in series (Figure 1B, shown in darker blue). Cells captured in the first trap will be released, filtered again using the second trap, and again using the third trap as shown in Figure 2 (Steps 1-4). Finally, all the trapped cells will be collected under high-pressure buffer flow when all the traps are opened (Figure 2, Step 5).

RESULTS AND DISCUSSION

Device Characterization using UM-UC13 cells. We used UM-UC13 bladder cancer cells doped into whole blood from healthy donors to characterize device performance and optimize process parameters. UM-UC13 cells and leukocytes have an overlapping size distribution, but significantly different deformabilities[21]. While the overlapping size-distribution limits the performance of size-only separation mechanisms, the RCT mechanism separates cells based on size and deformability. Thus, UM-UC13 cells are a good phenotype for validating the device by offering the distinct difference in deformability compared to leukocytes. Previously, we found that leukocyte contamination can be reduced by increasing the flow rate. However, at a flow rate of 4 mm s^{-1}, there appears to be irreversible damage to the trapped cancer cells because of the shear force applied to the cell membrane from the fluid [21]. Therefore, to minimize the potential damage to target cells, cell separation was performed at a flow rate of 2.5 mm s^{-1}.

For multi-filtration using three identical cell traps in parallel, the first trap acts as the initial filtration trap. To validate the multi-filtration process, cells filtered away during each filtration step and cells collected in the final collection step were directed and collected into different wells. The numbers of UM-UC13 cells and leukocytes in each well were counted to calculate the enrichment and yield of our RCT device at each step.

Figure 3A shows the enrichment and yield from a single filtration step. UC13 cells were doped into diluted whole blood at 1:1000 ratio to leukocytes. After processing a total of 15 samples, we found that that the first trap processed $2x10^6$ nucleated cells/hour with an average of 183-fold enrichment and 93.8% yield (Figure 3A). The yield results for doped UC13 cells are shown as a calibration curve in Figure 3B. Figure 3C shows results from a separate experiment to measure the enrichment and yield from multiple filtration steps. UC13 cells were doped at 1:1000 ratio to leukocytes too. Cells captured in the first trap were released and re-filtered through the second and third traps. The second and third traps together

provided an additional enrichment of ~5X without additional change in the yield (Figure 3B). The average enrichment of the third trap was 1.4. The enrichment performance of the RCT device was highly donor dependent but the trend of improvement was the same for each donor. These results show that the leukocytes that are captured in our device because of non-specific adhesion can be depleted by multiple re-filtrations. We achieved an average enrichment of ~900 after three filtrations, which rival previously reported label-free separation techniques [27–30].

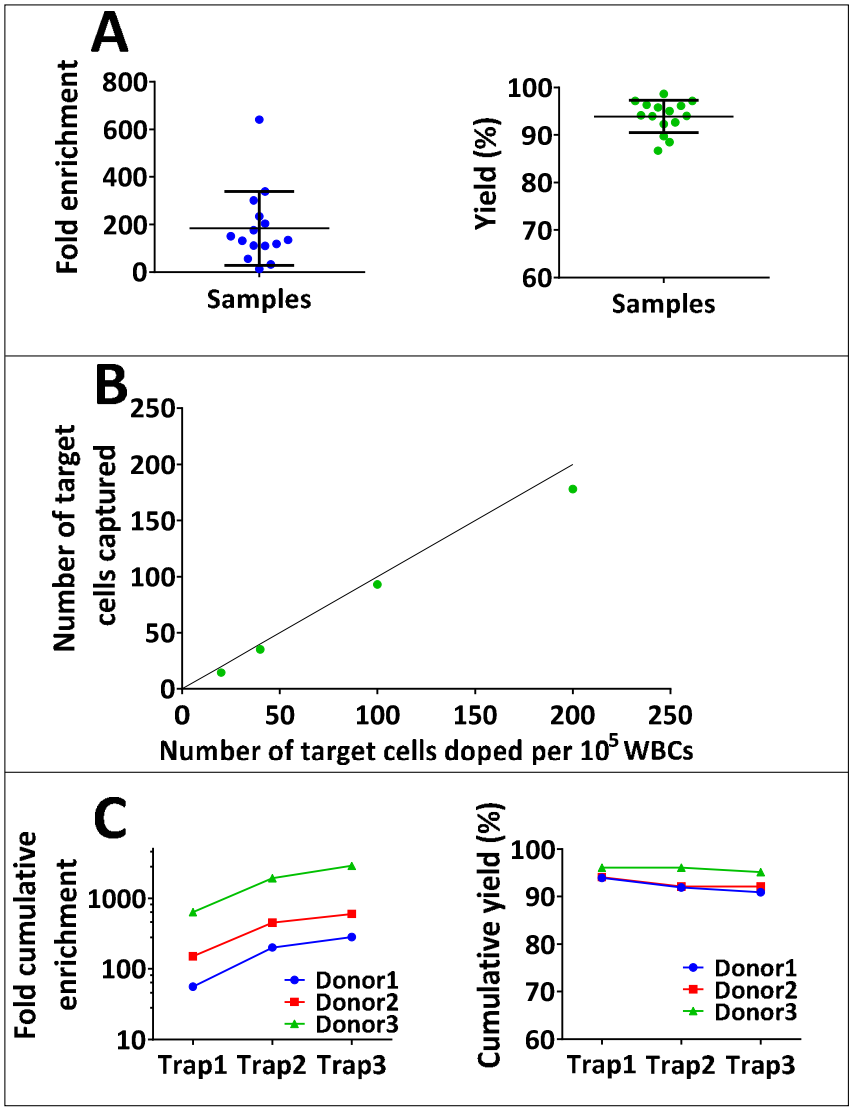

Figure 3: Performance of resettable cell traps in enrichment and retention of UM-UC13 cells relative to leukocytes. A: results of main filtration step from 15 samples (mean ± standard deviation). B: Calibration curve for the RCT mechanism. C: cumulative enrichment and yield results of 3-trap serial filtrations.

Device Characterization using LNCaP Cells. To further optimize parameters for processing samples from patients with prostate cancer, androgen-sensitive human prostate adenocarcinoma cells were used to characterize the device**.** Although cultured LNCaP cells have similar size distributions as the cultured UM-UC13 cells, they required a smaller trap opening, obtained through the application of a higher pressure across the diaphragm, to achieve the same retention ratio as UM-UC13 cells during processing. Furthermore, the flow speed limit that they can withstand before they are damaged is 1.5 mm s^{-1}, much less compared to the limit of 4 mm s^{-1} for UM-UC13 cells. This implies that LNCaP cells are more deformable than UM-UC13 cells. Multiple filtrations for LNCaP cells worked the same as for UM-UC13 cells. The only difference was that the average enrichment of the initial filtration step was much lower (83-fold) due to the slower flow speed and smaller channel openings. Extra filtrations gave an average enrichment improvement of ~5X, as before. Purity of enriched doping samples can be calculated from the enrichment. We hypothesized that CTCs from patients with metastatic castration-resistant prostate cancer (mCRPC) would be more deformable than cultured cancer cells. Previous studies have correlated greater deformability with greater invasiveness[31,32]. CTCs are highly invasive, and are therefore likely to be more deformable. As we have showed, LNCaP cells are more deformable than UM-UC13 cells, and are likely to better mimic CTCs. The parameter settings described for processing LNCaP cells were therefore applied to the processing of patient samples.

Working with Whole Blood. In early experiments, the yield of doped cancer cells was low when whole blood was processed directly. Whole blood was thus diluted in buffer to reduce the sample cell density, which improved the yield, as shown in Figure 4A. To determine whether this improvement was caused by the diluted leukocyte concentration or diluted red blood cell (RBC) concentration, the relationship between the yield and leukocyte concentration was investigated first. We separated leukocytes from whole blood, re-suspended them at various concentrations and added LNCaP cells to each suspension at a ratio of 1 LNCaP cell to 1000 leukocytes. The lack of correlation between the yield and leukocyte concentration indicates that the performance is not necessarily related to leukocyte concentration (Figure 4B). It was therefore determined that high concentrations of red blood cells (RBCs) negatively influence the yield of target cells trapped. RBCs aggregate in the storing pockets (Figure 4C) and prevent

incoming target cells from getting trapped. Therefore, to balance the overall yield and throughput, which are sacrificed with dilution, we implemented a 2 times dilution for processing samples.

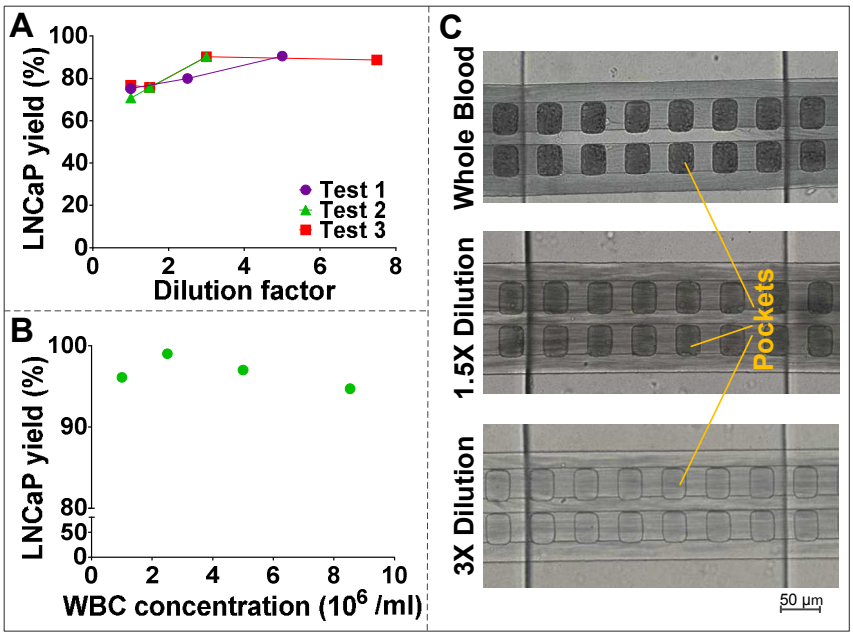

Figure 4: Parameter optimization of RCT devices for patient sample processing. A: LNCaP yield improved when whole blood was diluted. B: There was no correlation between the yield of LNCaP cells and the concentration of leukocytes. C: RBCs occupy the pockets at different densities when diluted.

Enrichment and identification of candidate CTCs from patients with mCRPC

Blood samples from 22 patients with mCRPC and 5 healthy controls were processed using the RCT device. After immunostaining and single-cell spectral analysis using the Zeiss LSM 780 system, enriched CTCs were defined as DAPI+ CK+ EpCAM+/- and CD45- while leukocytes were identified as DAPI+ CK- EpCAM- and CD45+ as represented in Figure 5A. The LSM 780 confocal microscopy system can simultaneously collect a 34-channel spectrum on each pixel of the image including a bright-field image, as well as a low wavelength channel for imaging the DAPI signal. Compared to standard fluorescent microscopy, which use individual color filters, this system provides greatly improved discrimination of overlapping emissions from multiple fluorophores. Our immunofluorescence system for CTC identification includes CK-Alexa 488 (emission peak at 529 nm), EpCAM-Alexa 594 (617 nm), and CD45-APC (660 nm). CTCs are distinguished from leukocytes based on the shape of their spectra. Typical CTCs and WBCs are shown in Figure 6B. A typical CTC spectrum has two distinct peaks: one for CK at 525 nm

and one for EpCAM at 617 nm. A typical spectrum of a leukocyte has only one clear peak for CD45 at 660 nm. A small amount of cells in the enriched samples were found to be positive for all 4 immunostains (Figure 5B) as reported previously by others[33]. The merged images of these cells look similar to CTCs, but can be distinguished by their spectral curves. As the nature of these cells is not yet established, they were not counted as CTC. The RCT device identified 81.8% (18/22) patients with >5 CTCs per 7.5ml of blood. The numbers varied between patients, from 0 to 930, with a mean of 257 per 7.5ml of blood. Within the same patient group, CellSearch analysis revealed >=5 CTCs in 40.9% (9/22) patients. The numbers ranged from 0 to 281 with a mean of 25 CTCs per 7.5 ml of blood. Control samples from five healthy donors were also processed with the RCT device. Scanned images of sorted cells of the healthy controls were mixed blindly with the images of patient samples and counted. Among the five healthy blind tests, only one donor had a count of 7.5 CTC per 7.5 ml of blood. The purity of enriched patient samples varies significantly since the number of CTCs varies dramatically from patient to patient. The number of leukocytes captured from 22 patient samples ranges from ~1,300 to ~18,000 per ml blood processed.

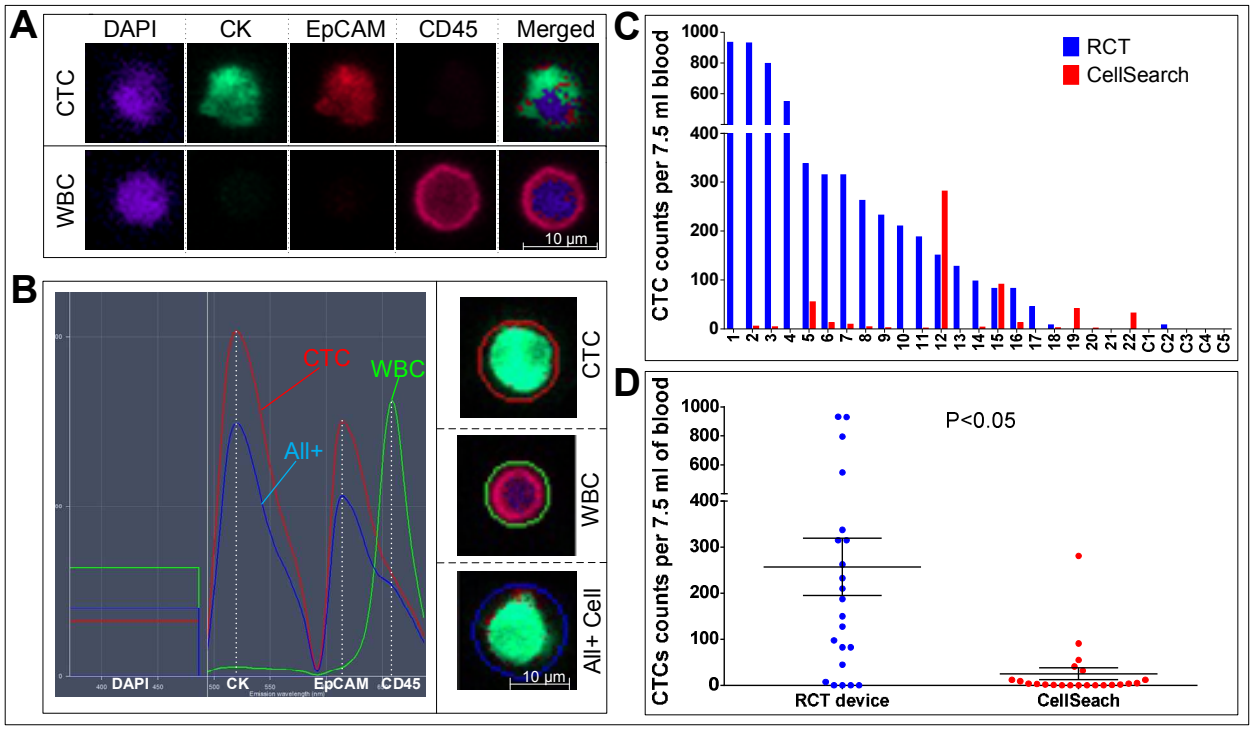

Figure 5: Enumeration of CTCs derived from CRPC patient samples. A: Micrographs of a CTC and leukocyte stained with fluorescent markers. B: Merged images of a CTC, a leukocyte and an all-positive

cell with their corresponding spectral curves. C: Number of CTCs identified following resettable cell trap (RCT) or CellSearch® enrichment. D: Grouped results of RCT device and CellSearch System. Data is displayed with mean ± standard deviation. P value is calculated by parametric paired T-test analysis. C1-C5 are normal controls.

As shown in Figure 5C and 5D, significantly more CTCs were identified using our approach compared to the CellSearch platform (p=0.0056). This improved capability derives from a combination of enhanced ability to capture CTCs, as well as a more sensitive an imaging system that permitted single cell spectral analysis. While these two aspects are necessarily coupled, we observe strong evidence that both contribute significantly to the overall increased sensitivity. Specifically, previous biomechanical (size and deformability) based separation approaches have demonstrate the ability to capture more CTCs compared to the EpCAM affinity capture method of the CellSearch System[33,34]. The discordance that we observed between the number of CTCs reported by CellSearch and the number reported by our enumeration system further suggests that our system is able to capture cells with low levels of EpCAM expression. From our single-cell spectral analysis, we also found high heterogeneity of expression levels (intensity of the spectrum) of markers for CTCs between patients. In 2/22 patient samples, EpCAM expression was much weaker than CK while the opposite was true for 3 of the other samples. There were also 4/22 patient samples with both weak CK and weak EpCAM expression. Interestingly, however, all CK+ CTCs identified using the RCT device were also EpCAM+, which likely arises from the greater sensitivity of the single cell spectral analysis technique. Previous reports affirmed that heterogeneity of biological properties (expression level of surface antigens) exist in CTCs from diverse cancer origins, different subtypes, and even the CTCs in the same patient[1,35]. The epithelial-to-mesenchymal transition (EMT) that occurs with dissemination of cancer cells into the blood stream results in down-regulation of EpCAM on the CTC surface [36,37]. For those samples with inadequate EpCAM expression, successful capture of CTCs may be impossible with the CellSearch system.

Coupling CTC enrichment using the RCT device with a single cell spectral analysis system provided both more sensitive and more objective discrimination of CTCs from contaminating leukocytes. This increased sensitivity derived in part from its spectral sensor, which has 1.8-fold higher quantum efficiency compared to conventional PMT detectors. This system is also more objective because it could accurately differentiate overlapping spectra. Classification of captured cells with the CellSearch system relies on an operators' judgment of the fluorescent images, where inconsistencies in the image interpretation may lead to incorrect identification of CTCs[38].

One potential concern for filtration-based separation of CTCs is the potential loss of smaller CTCs. Coumans and colleagues reported that the ideal diameter of a microsieve is 5 µm, which corresponds to the aperture adopted in this study[39]. However, these researchers and others have observed that CTC size varies from one tumor type to another[39,40]. A key advantage of the RCT mechanism is that the aperture of the device can be adapted dynamically altered to accommodate different tumor types. It would require further experimentation to determine the optimal aperture for CTCs derived from each tumor type but it is conceivable that careful optimization could enhance the performance of the device beyond what is presented in this report. The potential loss of smaller CTCs could result in an underestimation of the tumor cells in patient blood. However, prostate cancer has been reported to involve CTCs that are relatively small in size[39,40] and the observed sensitivity of RCT enrichment likely reflects the fact that even these small CTCs are significantly less deformable than contaminating leukocytes.

Overall, the performance of the RCT device competes well with other reported methods that process CRPC samples and the CellSearch system. Other methods are either based on EpCAM affinity capture [41–43] using EpCAM coated micro-structures which increase contact between CTC and surface and thereby improve efficiency, or are label-free methods based on the physical properties of CTCs [34,44] or even hybrid methods that combine both EpCAM affinity and the physical properties [45]. Unlike most label-free microfluidics chips, our RCT device can process whole blood samples with a dilution factor of only 2 [29,46]. There is no further processing of the blood sample such as lysis of RBCs [33,47] or fixation [34,48] where the addition of chemical buffers might affect the viability of the CTCs. Captured CTCs are easily retrieved from the collection reservoirs of the device for easy enumeration or further downstream analysis.

CONCLUSIONS

The RCT mechanism is a separation tool that enriches for CTCs from 2 x diluted whole blood with high throughput, sensitivity and selectivity. Furthermore, the RCT avoids the issue of clogging by the periodic resetting of its microstructures. We demonstrated the separation of viable, label-free CTCs from mCRPC patients, which were amenable to further standard cellular analysis methods, such as immunostaining. The RCT device presents a compelling and more sensitive alternative for the enrichment of CTCs based

on size and deformability that may enable better risk stratification and monitoring of treatment response in cancer patients.

MATERIALS AND METHODS

Fabrication and Set-up

The resettable cell trap (RCT) device was fabricated using standard multilayer soft lithography techniques using polydimethylsiloxane (PDMS) [22,49]. Master wafers for the control and flow layers are patterned through photolithography. Molds for the flow layer devices were fabricated using polyurethane and a master PDMS replica against the flow layer wafer. PDMS replicas against the master molds yielded the flow channels. The control channels were fabricated by coating a thin PDMS layer on the control layer wafers. These two layers were plasma bonded after they were separately oxidized in an oxygen plasma chamber (Harrick Plasma, Ithaca, NY). A 0.5 mm OD punch (Harris Unicore, Ted Pella Inc., Redding, CA) was used to create the inlet and outlet ports on-chip. Finally the device was plasma bonded to a 25x75 mm glass slide (Fisher Scientific).

Fluids flow into the device from 15 ml polypropylene falcon tubes (BD Biosciences, Mississauga, Canada) through Tygon microbore tubing with 0.02 inch inner diameter (ID) (Cole-Parmer, Montreal, Canada) and then a 0.017 inch ID stainless steel needle (New England Small Tube, Litchfield, NH) which is connected to the device. An external pneumatic pressure actuates the flow through custom machined caps fitted to the falcon tubes. The pneumatic pressure sources for sample and buffer infusion are offered by a 4-channel microfluidic flow control system (MCFS-Flex, Fluigent, France). The control valves on the device chip are activated by a custom designed system consisting of on-off pressure valves and a MSP430 microprocessor (Texas Instruments), which provides easy and flexible programming ability to meet different automation requirements. Prior to use, device channels were slowly flushed for 20 minutes with 0.2% Pluronic F-127 (Sigma-Aldrich, St. Louis, Missouri, USA) in PBC for surface passivation. Fluid outlets can be customized by either punching with a 6 mm outer diameter (OD) punch to form an on-chip reservoir or by punching with a 0.5 mm OD punch to lead out the fluids through needle and tubing to either a 96-well plate (Thermo Fisher Scientific, Rochester, NY, USA) or 15 ml tube.

The optimal trapping pressure for target cells was determined by following the target cells through a constricted trap and increasing the trapping pressure until over 90% of the target cells were captured.

The optical trapping pressure determined were 150 mbar for UC13 cells and 350 mbar for LNCaP cells (LNCaP cells are much softer than UC13 cells). For the validation experiments, where target cell concentration is specific, the processed volume in the first filtration step was based on a total of 100 target cells captured in the 128 channels or a total of 100,000 cells processed. This was to prevent obstruction of the flow channel, which will dramatically decrease the filtration ability. For processing patient samples, where the CTC and leukocytes concentration is unknown, conservative estimates are made to determine the length/volume of the main filtration. Patient samples processing utilizes the same parameter settings described for processing LNCaP cells: 350 mbar trapping pressure and 1.5 mm s^{-1} flow rate. This flow rate will yield a volumetric flow rate of 600 µl/h. Throughput is increased by further parallelization.

Sample Preparation

Device validation was performed using whole blood doped with UM-UC13 (provided by the Pathology Core of the Bladder Cancer SPORE at MD Anderson Cancer Center) bladder cancer cells and LNCaP prostate cancer cells (American Type Culture Collection (ATCC), Manassas, VA, USA). UC13 bladder cancer cells were cultured in complete minimal essential medium (CMEM): minimum essential medium Eagle (MEM) (Life Technology, Carlsbad, CA, USA) supplemented with 10% (v/v) fetal bovine serum (Life Technology), 1% sodium pyruvate (Invitrogen), 1% L-glutamine (Life Technology), 1% MEM non-essential amino acids (Life Technology), and 1% penicillin streptomycin (Fisher Scientific). LNCaP cells were cultured in RPMI 1640 media (Life Technology) containing 10% (v/v) fetal bovine serum, 2mM L-glutamine and 1% penicillin/streptomycin. Both cell lines were incubated in a humidified environment at 37°C and 5% CO_2. When needed, cells were trypsinized, washed and resuspended at the desired concentration for experiments.

After informed consent was received from healthy donors (n=20), whole blood was drawn into 6 ml EDTA collection tubes (Becton-Dickinson, Franklin Lakes, NJ, USA). Leukocytes in the whole blood were stained with Hoechst 33342 (Invitrogen, Carlsbad, CA, USA), which emits a blue fluorescence, and were further diluted to 2 million leukocytes per ml with phosphate buffered saline (PBS, Gibco).

For validation experiments, cancer cells, stained with Calcein AM (Invitrogen), which emits a green fluorescence, were doped into the whole blood which was diluted to $2x10^6$ leukocytes/ml. The mixed sample that was processed in each cell separation trial for validation experiments contained a minimum

of 100 cancer cells at different doping ratios. Each sample was processed in multiple full device operation cycles with each cycle processing ~100,000 leukocytes.

Experimental Characterization of the Device Performance

The yield and enrichment are the two main characteristics used to measure the performance of the RCT device. The yield is defined as the retention rate of target cells. The enrichment is defined as the ratio of target cancer cells to background cells in the collection reservoir divided by the same ratio of the input sample. To get these results, we counted the number of cancer cells in both collection and waste reservoirs and leukocytes (background cells) in the collection reservoir after each experiment. Cancer cells were identified by the green fluorescence of the Calcein AM stain and the leukocytes were blue from the Hoescht 33342 stain. Images were taken using an inverted microscope with fluorescent capabilities (Nikon ECLIPSE Ti) and camera (QImaging, Surrey, BC, Canada). The numbers of cells in the images were manually counted.

Patient Blood Sample Acquisition, Separation, Immunofluorescence, and Enumeration

Patients with metastatic castrate resistant prostate cancer (n=22) were recruited at the BC Cancer Agency. This study was approved by the institutional review board (protocol H13-00870). After informed consent was obtained, blood samples were collected in 6 ml EDTA tubes (BD). The CRPC patients in this study ranged in age from 49–88 years, had PSA levels between 0.05 and 12,840 µg/L. Each 1 ml of blood was diluted 1:1 with PBS in a 15 ml falcon tube. The diluted sample was directly processed with the RCT device. A parallel sample of 7.5 ml of blood was analyzed using the Veridex CellSearch™ system.

The cells were collected into a 15 ml falcon tube through needle and microbore tubing. The enriched cell fraction was washed with 1 x PBS, centrifuged at 400 g for 5 min and then fixed in 3% paraformaldehyde (PFA, Sigma, USA) for 15 min. After fixation, the cells were permeabilized in 0.5% Tween20 for 10 min, washed in PBS, and blocked by incubation with 3% BSA (Sigma-Aldrich, St. Louis, Missouri, USA) in PBS for 30 min and washed a final time in PBS. Every step was conducted at room temperature. Cells were stained with antibodies for cytokeratin (CK) using Pan-Keratin (C11) Mouse mAb-Alexa Fluor® 488 (Cell Signaling Technology, Danvers, Massachusetts, USA), EpCAM (VU1D9) Mouse mAb-Alexa Fluor® 594 (Cell Signaling Technology), and anti-human CD45-APC (Biolegend, San Diego, California, USA) at 0.625 µg/ml, 0.525 µg/ml, 0.36 µg/ml respectively in PBS/3% BSA at 4°C overnight.

Stained cells were washed 3 times with PBS to remove floating superfluous antibodies. After the last centrifuge, cells were suspended in 40ul PBS and stained with DAPI using VECTASHIELD® Mouting medium with DAPI (Vector Laboratories, Burlingame, CA, USA) at a concentration of 0.075 µg/ml. All cells were transferred to a single well of a Corning® 384-well high content image plate (Sigma-Aldrich) and centrifuged at 400 g for 2 min. The well was automatically scanned at 40X magnification with a confocal microscope (LSM 780, Carl Zeiss, Oberkochen, Germany) and Zen software (Carl Zeiss). Spectrum analysis of single cells was manually conducted to identify the presence of CTCs candidates. DAPI+/CK+/EpCAM+or-/CD45- enriched cells were considered CTCs while DAPI+/CK-/EpCAM-/CD45+ enriched cells were considered WBCs. CTCs counts from the RCT device were scaled to numbers per 7.5 ml to compare with the CellSearch system.

ACKNOWLEDGEMENT

This work was made possible by grants from Natural Sciences and Engineering Research Council of Canada Canadian Institutes of Health Research, Prostate Cancer Canada, Vancouver Prostate Centre's Translational Research Initiative for Accelerated Discovery and Development, C.J. Martin Biomedical Overseas Fellowship from the National Health and Medical Research Council of Australia, and Engineers-in-Scrubs training program at UBC.

REFERENCES

1 A. van de Stolpe, K. Pantel, S. Sleijfer, L. W. Terstappen and J. M. J. den Toonder, *Cancer Res.*, 2011, **71**, 5955–5960.
2 E. S. Lianidou, A. Strati and A. Markou, *Crit. Rev. Clin. Lab. Sci.*, 2014, **51**, 160–171.
3 A. E. Dago, A. Stepansky, A. Carlsson, M. Luttgen, J. Kendall, T. Baslan, A. Kolatkar, M. Wigler, K. Bethel, M. E. Gross, J. Hicks and P. Kuhn, *PloS One*, 2014, **9**, e101777.
4 D. F. Hayes, M. Cristofanilli, G. T. Budd, M. J. Ellis, A. Stopeck, M. C. Miller, J. Matera, W. J. Allard, G. V. Doyle and L. W. Terstappen, *Clin. Cancer Res.*, 2006, **12**, 4218–4224.
5 J. S. de Bono, H. I. Scher, R. B. Montgomery, C. Parker, M. C. Miller, H. Tissing, G. V. Doyle, L. W. Terstappen, K. J. Pienta and D. Raghavan, *Clin. Cancer Res.*, 2008, **14**, 6302–6309.
6 S. J. Cohen, C. J. Punt, N. Iannotti, B. H. Saidman, K. D. Sabbath, N. Y. Gabrail, J. Picus, M. Morse, E. Mitchell and M. C. Miller, *J. Clin. Oncol.*, 2008, **26**, 3213–3221.
7 X.-L. Ma, Y.-Y. Li, J. Zhang, J.-W. Huang, H.-Y. Jia, L. Liu and P. Li, *Asian Pac. J. Cancer Prev. APJCP*, 2014, **15**, 6015–6020.
8 A. Kulasinghe, C. Perry, L. Jovanovic, C. Nelson and C. Punyadeera, *Int. J. Cancer J. Int. Cancer*, 2015, **136**, 2515–2523.
9 C. Jin, S. M. McFaul, S. P. Duffy, X. Deng, P. Tavassoli, P. C. Black and H. Ma, *Lab. Chip*, 2014, **14**, 32–44.

10 S. Riethdorf, H. Fritsche, V. Müller, T. Rau, C. Schindlbeck, B. Rack, W. Janni, C. Coith, K. Beck, F. Jänicke, S. Jackson, T. Gornet, M. Cristofanilli and K. Pantel, *Clin. Cancer Res. Off. J. Am. Assoc. Cancer Res.*, 2007, **13**, 920–928.

11 S. Nagrath, L. V. Sequist, S. Maheswaran, D. W. Bell, D. Irimia, L. Ulkus, M. R. Smith, E. L. Kwak, S. Digumarthy, A. Muzikansky, P. Ryan, U. J. Balis, R. G. Tompkins, D. A. Haber and M. Toner, *Nature*, 2007, **450**, 1235–1239.

12 M. Lin, J.-F. Chen, Y.-T. Lu, Y. Zhang, J. Song, S. Hou, Z. Ke and H.-R. Tseng, *Acc. Chem. Res.*, 2014, **47**, 2941–2950.

13 V. Murlidhar, M. Zeinali, S. Grabauskiene, M. Ghannad-Rezaie, M. S. Wicha, D. M. Simeone, N. Ramnath, R. M. Reddy and S. Nagrath, *Small Weinh. Bergstr. Ger.*, 2014, **10**, 4895–4904.

14 A. A. Powell, A. H. Talasaz, H. Zhang, M. A. Coram, A. Reddy, G. Deng, M. L. Telli, R. H. Advani, R. W. Carlson, J. A. Mollick, S. Sheth, A. W. Kurian, J. M. Ford, F. E. Stockdale, S. R. Quake, R. F. Pease, M. N. Mindrinos, G. Bhanot, S. H. Dairkee, R. W. Davis and S. S. Jeffrey, *PloS One*, 2012, **7**, e33788.

15 N. Krawczyk, F. Meier-Stiegen, M. Banys, H. Neubauer, E. Ruckhaeberle and T. Fehm, *BioMed Res. Int.*, 2014, **2014**, 415721.

16 S. J. Tan, R. L. Lakshmi, P. Chen, W.-T. Lim, L. Yobas and C. T. Lim, *Biosens. Bioelectron.*, 2010, **26**, 1701–1705.

17 S. Zheng, H. Lin, J.-Q. Liu, M. Balic, R. Datar, R. J. Cote and Y.-C. Tai, *J. Chromatogr. A*, 2007, **1162**, 154–161.

18 Y. Tang, J. Shi, S. Li, L. Wang, Y. E. Cayre and Y. Chen, *Sci. Rep.*, 2014, **4**, 6052.

19 R. A. Harouaka, M.-D. Zhou, Y.-T. Yeh, W. J. Khan, A. Das, X. Liu, C. C. Christ, D. T. Dicker, T. S. Baney, J. T. Kaifi, C. P. Belani, C. I. Truica, W. S. El-Deiry, J. P. Allerton and S.-Y. Zheng, *Clin. Chem.*, 2014, **60**, 323–333.

20 T. Gerhardt, S. Woo and H. Ma, *Lab. Chip*, 2011, **11**, 2731–2737.

21 W. Beattie, X. Qin, L. Wang and H. Ma, *Lab. Chip*, 2014, **14**, 2657–2665.

22 M. A. Unger, H. P. Chou, T. Thorsen, A. Scherer and S. R. Quake, *Science*, 2000, **288**, 113–116.

23 S.-B. Huang, M.-H. Wu and G.-B. Lee, *Sens. Actuators B Chem.*, 2009, **142**, 389–399.

24 L. Saias, J. Autebert, L. Malaquin and J.-L. Viovy, *Lab. Chip*, 2011, **11**, 822–832.

25 A. Jain and L. L. Munn, *PLoS ONE*, 2009, **4**, e7104.

26 S. K. Murthy, A. Sin, R. G. Tompkins and M. Toner, *Langmuir ACS J. Surf. Colloids*, 2004, **20**, 11649–11655.

27 J. Sun, M. Li, C. Liu, Y. Zhang, D. Liu, W. Liu, G. Hu and X. Jiang, *Lab. Chip*, 2012, **12**, 3952–3960.

28 H. S. Moon, K. Kwon, K. A. Hyun, T. Seok Sim, J. Chan Park, J. G. Lee and H. I. Jung, *Biomicrofluidics*, 2013, **7**, 14105.

29 S. Zheng, H. K. Lin, B. Lu, A. Williams, R. Datar, R. J. Cote and Y.-C. Tai, *Biomed. Microdevices*, 2011, **13**, 203–213.

30 S. C. Hur, A. J. Mach and D. Di Carlo, *Biomicrofluidics*, 2011, **5**, 22206.

31 V. Swaminathan, K. Mythreye, E. T. O'Brien, A. Berchuck, G. C. Blobe and R. Superfine, *Cancer Res.*, 2011, **71**, 5075–5080.

32 J. Guck, S. Schinkinger, B. Lincoln, F. Wottawah, S. Ebert, M. Romeyke, D. Lenz, H. M. Erickson, R. Ananthakrishnan, D. Mitchell, J. Käs, S. Ulvick and C. Bilby, *Biophys. J.*, 2005, **88**, 3689–3698.

33 B. L. Khoo, M. E. Warkiani, D. S.-W. Tan, A. A. S. Bhagat, D. Irwin, D. P. Lau, A. S. T. Lim, K. H. Lim, S. S. Krisna, W.-T. Lim, Y. S. Yap, S. C. Lee, R. A. Soo, J. Han and C. T. Lim, *PLoS ONE*, 2014, **9**, e99409.

34 H. K. Lin, S. Zheng, A. J. Williams, M. Balic, S. Groshen, H. I. Scher, M. Fleisher, W. Stadler, R. H. Datar, Y.-C. Tai and R. J. Cote, *Clin. Cancer Res.*, 2010, **16**, 5011–5018.

35 A. M. Sieuwerts, J. Kraan, J. Bolt, P. van der Spoel, F. Elstrodt, M. Schutte, J. W. M. Martens, J.-W. Gratama, S. Sleijfer and J. A. Foekens, *J. Natl. Cancer Inst.*, 2009, **101**, 61–66.

36 C. G. Rao, D. Chianese, G. V. Doyle, M. C. Miller, T. Russell, R. A. Sanders and L. W. M. M. Terstappen, *Int. J. Oncol.*, 2005, **27**, 49–57.

37 O. Gires and N. H. Stoecklein, *Cell. Mol. Life Sci. CMLS*, 2014, **71**, 4393–4402.

38 J. Kraan, S. Sleijfer, M. H. Strijbos, M. Ignatiadis, D. Peeters, J.-Y. Pierga, F. Farace, S. Riethdorf, T. Fehm, L. Zorzino, A. G. J. Tibbe, M. Maestro, R. Gisbert-Criado, G. Denton, J. S. de Bono, C. Dive, J. A. Foekens and J. W. Gratama, *Cytometry B Clin. Cytom.*, 2011, **80B**, 112–118.

39 F. A. W. Coumans, G. van Dalum, M. Beck and L. W. M. M. Terstappen, *PloS One*, 2013, **8**, e61770.

40 S. T. Ligthart, F. A. W. Coumans, F. C. Bidard, L. H. J. Simkens, C. J. A. Punt, M. R. de Groot, G. Attard, J. S. de Bono, J.-Y. Pierga and L. W. M. M. Terstappen, *PloS One*, 2013, **8**, e67148.

41 S. Wang, K. Liu, J. Liu, Z. T.-F. Yu, X. Xu, L. Zhao, T. Lee, E. K. Lee, J. Reiss, Y.-K. Lee, L. W. K. Chung, J. Huang, M. Rettig, D. Seligson, K. N. Duraiswamy, C. K.-F. Shen and H.-R. Tseng, *Angew. Chem. Int. Ed.*, 2011, **50**, 3084–3088.

42 T. W. Friedlander, V. T. Ngo, H. Dong, G. Premasekharan, V. Weinberg, S. Doty, Q. Zhao, E. G. Gilbert, C. J. Ryan, W.-T. Chen and P. L. Paris, *Int. J. Cancer J. Int. Cancer*, 2014, **134**, 2284–2293.

43 S. L. Stott, C.-H. Hsu, D. I. Tsukrov, M. Yu, D. T. Miyamoto, B. A. Waltman, S. M. Rothenberg, A. M. Shah, M. E. Smas, G. K. Korir, F. P. Floyd, A. J. Gilman, J. B. Lord, D. Winokur, S. Springer, D. Irimia, S. Nagrath, L. V. Sequist, R. J. Lee, K. J. Isselbacher, S. Maheswaran, D. A. Haber and M. Toner, *Proc. Natl. Acad. Sci.*, 2010, **107**, 18392–18397.

44 F. Farace, C. Massard, N. Vimond, F. Drusch, N. Jacques, F. Billiot, A. Laplanche, A. Chauchereau, L. Lacroix, D. Planchard, S. Le Moulec, F. André, K. Fizazi, J. C. Soria and P. Vielh, *Br. J. Cancer*, 2011, **105**, 847–853.

45 E. Ozkumur, A. M. Shah, J. C. Ciciliano, B. L. Emmink, D. T. Miyamoto, E. Brachtel, M. Yu, P. Chen, B. Morgan, J. Trautwein, A. Kimura, S. Sengupta, S. L. Stott, N. M. Karabacak, T. A. Barber, J. R. Walsh, K. Smith, P. S. Spuhler, J. P. Sullivan, R. J. Lee, D. T. Ting, X. Luo, A. T. Shaw, A. Bardia, L. V. Sequist, D. N. Louis, S. Maheswaran, R. Kapur, D. A. Haber and M. Toner, *Sci. Transl. Med.*, 2013, **5**, 179ra47–179ra47.

46 E. Sollier, D. E. Go, J. Che, D. R. Gossett, S. O'Byrne, W. M. Weaver, N. Kummer, M. Rettig, J. Goldman, N. Nickols, S. McCloskey, R. P. Kulkarni and D. Di Carlo, *Lab. Chip*, 2014, **14**, 63–77.

47 L. T. D. Chinen, C. A. L. Mello, E. A. Abdallah, L. M. Ocea, M. E. Buim, N. M. Breve, J. L. Gasparini, M. F. Fanelli and P. Paterlini-Bréchot, *OncoTargets Ther.*, 2014, **7**, 1609–1617.

48 R. RIAHI, P. GOGOI, S. SEPEHRI, Y. ZHOU, K. HANDIQUE, J. GODSEY and Y. WANG, *Int. J. Oncol.*, 2014, **44**, 1870–1878.

49D. C. Duffy, J. C. McDonald, O. J. A. Schueller and G. M. Whitesides, *Anal. Chem.*, 1998, **70**, 4974–4984.